

Development of a Low Cost Sensored Control for High-Speed Axial Flux Permanent Magnet Machines

Dr. Tareq El-Hasan^{1*} Eng. Mahmoud Elnasser²

1. Vice Dean Faculty of Engineering Technology, Zarqa University 132222, Zarqa 13132, Jordan

2. Executive Manager, Elnasser Electronics CO. Amman, Jordan

* E-mail: tareq.elhasan@zu.edu.jo

This research is funded by the Deanship of Research and Graduate Studies in Zarqa University /Jordan

Abstract

A Low Cost Control for a compact High-Power High-Speed Axial Flux Permanent Magnet (AFPM) Machine has been developed in this research. The machine under consideration has been designed to run in the generation as well as in the motoring mode for utilization in vast industrial and automotive applications. When used as a motor for automotive applications, the machine is directly coupled to a radial inward flow compressor to operate as an electric driven supercharger running in the range of 40,000 – 50,00 rpm. To run the machine as a motor at its rated speed and power, a suitable electric drive and controller has to be utilized while considering the machine performance characteristics. Most of the available Commercial Off-The-Shelf (COTS) systems are either designed for low-speed high-power machines or high-speed, low-power machines. In addition, the self inductance of such machines are relatively high (in the range of hundreds of millihenry) compared to the AFPM machine under consideration which has a very low self inductance (in the range of tens of microhenry). The low inductance of PM machines often makes current control difficult. If high switching frequencies are not used, the current ripple in the machine windings will be very high, causing degradation of the overall machine efficiency and increasing the rotor torque ripple and pulsation. In this research a high frequency inverter-based controllers using Insulated Gate Bipolar Transistors (IGBTs) is utilized to overcome the problem of the low inductance of the machine. For simple and low cost control scheme, Hall effect sensors are used to energize the machine coils in the appropriate sequence thus providing accurate and precise control. The sensored control is analyzed using computer simulation and a prototype of the controller is also developed. Simulation results are validated by the experimental tests which showed good match and demonstrated the machine behavior under such controller and provided promising results for further research and investigations.

Keywords: sensored control, low cost control, permanent magnet machines, axial flux machines;

1. Introduction

Permanent Magnet (PM) machines are increasingly becoming dominant machines with the cost competitiveness of high energy PM. These machines offer many unique features as they are usually more efficient because the field excitation losses are eliminated resulting in significant rotor loss reduction.

Since the introduction of high energy magnets, a number of papers have been published on the design and construction of High-speed PM machines [1], [2]. Most recently, some of these designs demonstrated the potential and advantages of AFPM Machines with a single central stator with magnets mounted on rotors on either side [3] and [4].

AFPM machines can be developed for high speed applications if special arrangement and several precautions are taken into consideration such as:

- Adaptation of starting and control strategies of the machines
- Minimizing rotor losses and consideration of cooling aspects for stator windings and rotor
- Elimination of vibration and mechanical problems

Most published research activities on the control of high speed PM machines have been focused on low-power application (fraction of kW) [5], [6] and [7]. In this paper, a simple, low cost sensored control for high-power (10s kW), high-speed AFPM machine is presented as it is required to understand the machine's behavior and validate the simulation models before proceeding with sensorless control. Although sensored control is simpler to develop, sensorless control provides some benefits over the sensored control due the absence of sensing elements. Therefore the results from this research can be used as a baseline for further research to develop a rugged, reliable and efficient control for such types of machines. In addition, the effect of machine's parameters, such as low coil inductance and mutual inductances effect on the machine behavior can be accurately examined at earlier stages of the development of the advanced model for the control of the high-speed AFPM machine.

2. Machine Description

Axial Flux machines are different from conventional electrical machines in terms of the direction of the flux which runs parallel with the mechanical shaft of the machine. The current flowing through each stator coil

interacts with the flux created by the magnets on the rotor, producing a force tangential to the rotor circumference. Despite the large variety in the existing AFPM machines, it is still possible to mention some common features which can be categorized as advantages with respect to conventional electrical machines such as compactness, high efficiency and simple manufacturing. An example of the HS AFPM machine under investigation in this paper is depicted in **Figure 1**. Whereas the three phase windings of the machine with the hall sensors integrated is shown in **Figure 2**.



Figure 1: High Speed AFPM Machine under consideration

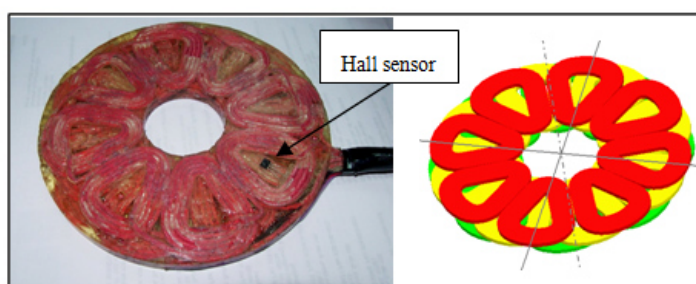


Figure 2: Three-phase windings of the AFPM machine with Hall sensor

3. Machine Characteristics

Before starting the modeling and simulation processes, it is necessary to understand the principles of the machine and to determine the problems in controlling such types of machines. The low winding inductances are a typical feature of the ironless AFPM machines. This makes the design of the current control system for such machines critical since it requires higher switching frequencies. The main characteristics of the machine under consideration for this research are presented in **Table I**.

Table I: AFPM main characteristics

Parameters	Value	Unit
Maximum speed	50,000	RPM
Number of phases	3	-
Weight	2.5	Kg
Rated Power	18	kVA
Load torque	4	N.m
Winding resistance	6	mΩ
Stator self inductance	80	μH
Rotor flux	7.5	mWb
Number of pole pair	4	-
Rotor moment of inertia	30.25	Kg.cm ²

4. Machine Modeling

4.1 Modeling of the High-Speed AFPM Machine

In this paper an 8-pole AFPM machine, with three-phase stator windings generating trapezoidal back EMF is considered for the machine model. Therefore ABC phase variable model is favored on the d-q axis transformation. The following assumptions are made for the machine model:

- No saturation effect since the stator has an ironless design.
- Stator resistance, self-inductance of all phases are equal and constant.
- Mutual inductances are very small therefore can be neglected.
- Hysteresis and eddy current losses are eliminated.

- All semiconductor switches are ideal.

The electrical mathematical equations of the AFPM machine are:

$$v_a = R_s i_a + L_s \frac{di_a}{dt} + E_a \quad (1)$$

$$v_b = R_s i_b + L_s \frac{di_b}{dt} + E_b \quad (2)$$

$$v_c = R_s i_c + L_s \frac{di_c}{dt} + E_c \quad (3)$$

By re-arranging equations (1), (2) and (3) the electrical equations can be defined as [8, 9]:

$$\frac{d}{dt} i_a = \frac{1}{3L_s} (2v_{ab} + v_{bc} - 3R_s i_a + \lambda p \omega_r (-2E_a + E_b + E_c)) \quad (4)$$

$$\frac{d}{dt} i_b = \frac{1}{3L_s} (-v_{ab} + v_{bc} - 3R_s i_b + \lambda p \omega_r (E_a - 2E_b + E_c)) \quad (5)$$

$$\frac{d}{dt} i_c = -\left(\frac{d}{dt} i_a + \frac{d}{dt} i_b \right) \quad (6)$$

$$E_{a,b,c} = K \lambda \omega_r \quad (7)$$

Where:

L_s ; Inductance of the stator windings

R_s ; Resistance of the stator windings

i_a, i_b, i_c ; a, b and c phase currents

v_{ab}, v_{bc} ; ab and bc phase to phase voltages

ω_r ; Angular velocity of the rotor

λ ; Amplitude of the flux induced by the permanent magnets of the rotor in the stator phases

p ; Number of pole pairs

K :Machine's electrical constant.

E_a, E_b, E_c ; a, b and c are phase trapezoidal electromotive forces and their waveforms can be graphically represented as shown in **Figure 3**.

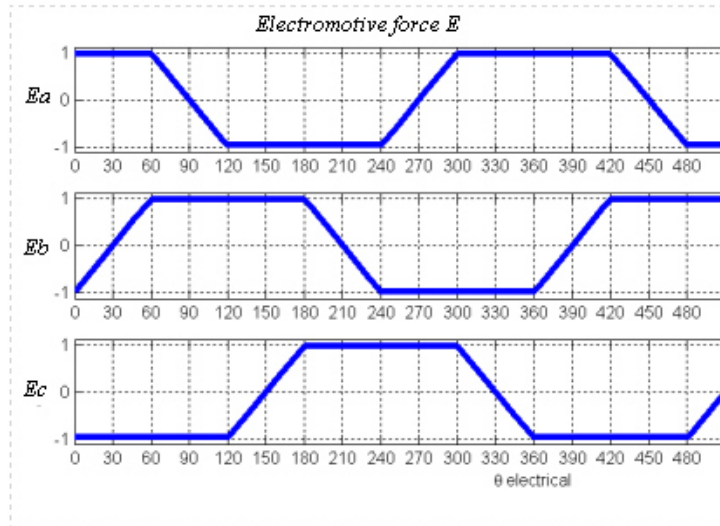


Figure 3: Representation of 3-phase trapezoidal electromotive forces

4.2 Torque Expression of the AFPM Machine

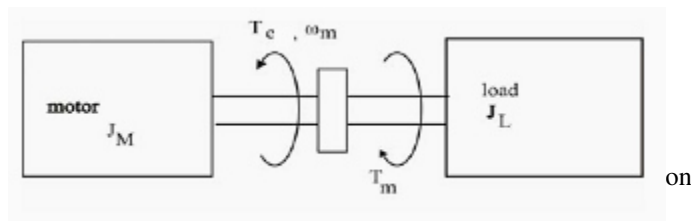
The expression for the electromagnetic torque developed by the machine can be obtained from the component of the input power (P) that is transferred across the air gap. Hence the electromechanical torque can be obtained as:

$$T_e = P \lambda (E_a \cdot i_a + E_b \cdot i_b + E_c \cdot i_c) \quad (8)$$

The relationship between the electromechanical torque and the load torque is given as:

$$T_e = J_m \frac{d\omega_r}{dt} + T_l + F \omega_r \quad (9)$$

Under load condition, the motor under consideration can be represented as shown in **Figure 4**.



Hence, the mechanical system can be defined by the following equations:

$$\frac{d}{dt} \omega_r = \frac{1}{J} (T_e - T_f - F \omega_r - T_m) \quad (10)$$

$$\frac{d\theta}{dt} = \omega_r \quad (11)$$

Where:

- $J = J_M + J_L$; is the combined inertia of rotor and load
- F ; Combined viscous friction of rotor and load
- θ ; Rotor angular position
- T_m ; Shaft mechanical torque
- T_f ; Shaft static friction torque
- P ; Input power transferred through the air gap

5. Controller and Inverter Design Description

To run the AFPM machine as a motor, it is fed through a three leg inverter with the DSP gate drive fed through Hall sensors. The overall block diagram of the proposed inverter and control circuit is depicted in **Figure 5**. The control circuit and inverter consist of four main sections which are described below.

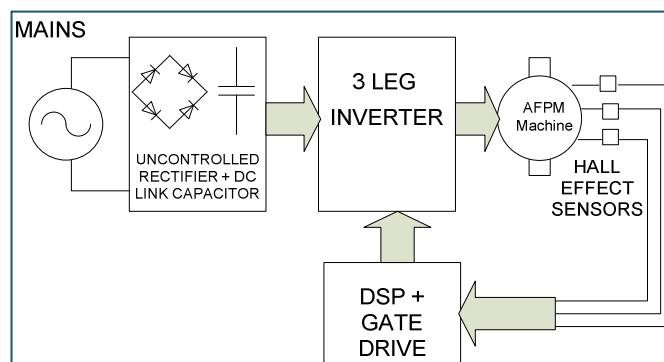


Figure 5: Block diagram for the proposed sensorless control strategy

5.1 Uncontrolled Bridge Rectifier and DC Link Capacitor (filter)

This section is used to rectify the non-isolated mains voltage and smooth it with the DC-Link capacitor to supply the high speed AFPM machine with DC voltage and act as a reservoir for regenerative braking of the machine. The power diodes should be capable of withstanding both the peak line voltage with safety margin in case of regeneration, and the maximum expected load current. For a supply voltage of 220v rms, the peak line voltage is therefore determined as:

$$V_{Line(pk)} = 220\sqrt{2} = 311 \text{ VDC}; \text{ where mains supply AC voltage is } 220 \text{ VAC at } 50\text{Hz.}$$

During regenerative braking, the DC supply voltage can rise above $V_{Line(pk)}$. If the permitted rise is 50%, the diodes should be capable of withstanding at least 470VDC and carrying the maximum allowable motor current.

5.2 Inverter Power Circuit

It consists of a 6-pack IGBT module SKM40GD123 from Semikron with built in fast recovery free-wheeling diodes connected in anti-parallel with IGBTs as seen in **Figure 6** to make design compact and easier for installation.

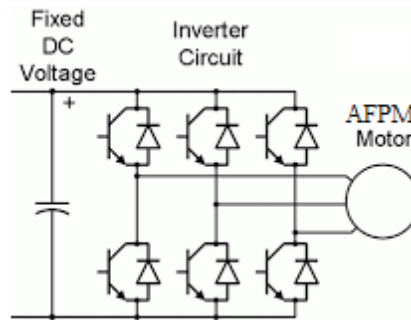


Figure 6: Six pack IGBT with integrated free-wheeling diodes

5.3 IGBT Gate Drive

This section is required to charge the IGBT's gate capacitance and discharge it quickly to reduce switching losses and increase efficiency. The gate drive circuit must be capable of supplying sufficient current to charge this capacitance during turn on in the shortest possible time. During turn off the gate drive circuit has to discharge the capacitance rapidly, and it must therefore have very low sink impedance. These conditions ensure that turn-on and turn-off times are both very short, and the switching losses are consequently small. That's the reason for selecting a dedicated floating channel high and low side driver IC IR2112 optimized for MOSFET and IGBT gate drive application. This IC works on bootstrap principle to simplify the design of high sides IGBT drive power supply requirements eliminating the need for extra isolated power supplies for each high side IGBT. The schematics for one leg gate drive repeated to control the other two legs is depicted in **Figure 7**.

5.4 Control Section

This is based on Microchip's dsPIC30F2010 Digital Signal Controller. This Microchip provides a single chip solution for position sensing, speed and direction control which can be varied by a speed demand input potentiometer, connected to analog to digital converter (ADC) input. It also has a dedicated 6 channel PWM motor control module designed to control the 6 IGBTs by hardware with built in dead time control to free the software control from the burden of calculating dead time and to allow for more efficient control algorithms. The schematic diagram for DSP controller and gate drive is shown in **Figure 8**. It is worth mentioning that the three Hall effect sensor outputs are connected to the input pins of the dsPIC that have Change Notification circuits associated with them. These inputs are enabled with their interrupt. If a change occurs on any of these three pins, an interrupt is generated and switching sequence of the 3 phase coils is changed accordingly improving efficiency and making rigor control on the sensed AFPM machine.

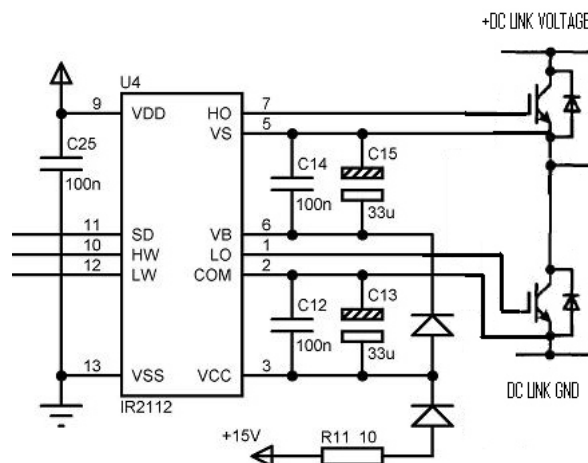


Figure 7: Schematics for one leg gate driver using IC (IR2112)

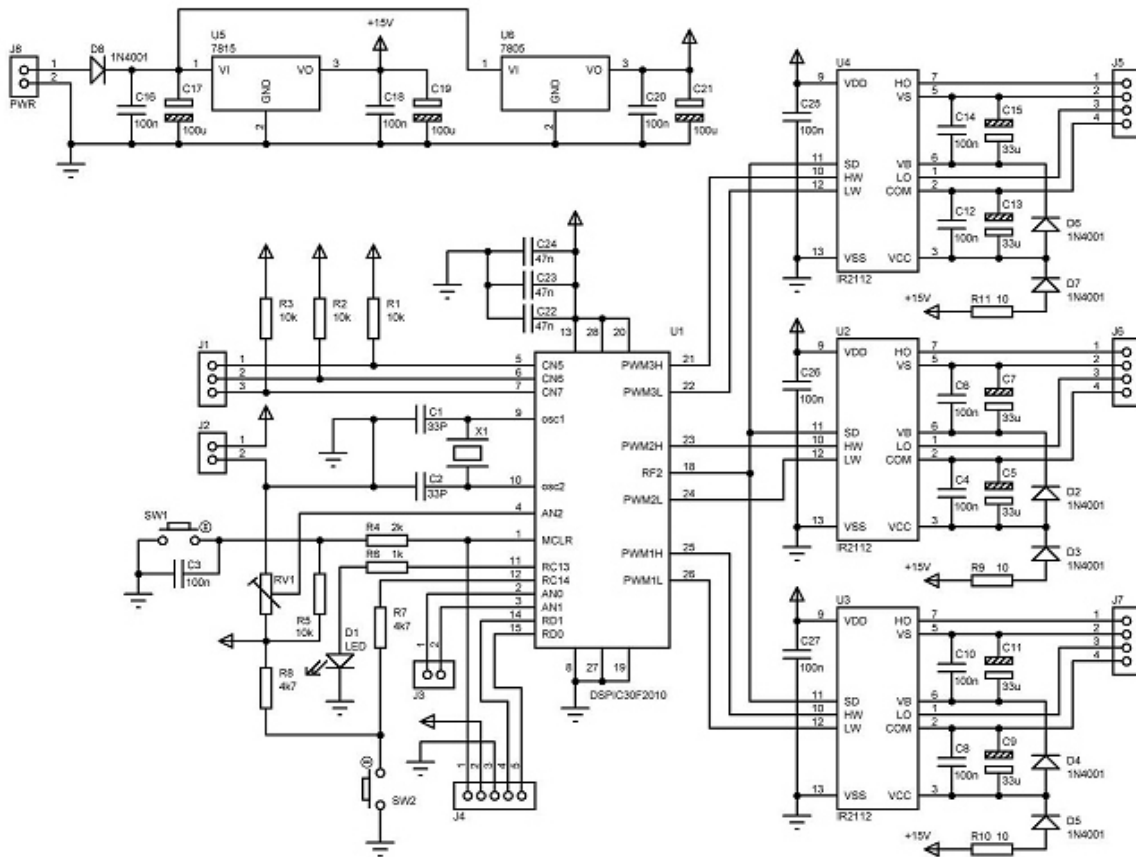


Figure 8: Schematics of DSP board and gate drive circuit

6. Software Design Description SDD

Open-Loop control was implemented at this stage for the purpose of simplification of the investigation of the high speed AFPM machine behavior under such a control strategy. In this scheme, the dsPIC controls the motor speed based on the voltage input from the speed pot using PWM technique. After power is set on, the dsPIC initializes PWM registers, ADC, ports and the Change Notification inputs. Once the start push button is activated, Hall effect sensors are read based on the rotor position and a corresponding value is retrieved from the table and written to the IGBTs gate drive circuitry which enable the motor to start running at a specific direction. Flowcharts of the open loop control software and Change Notification Interrupts of Hall effect sensors are shown in Figure 9 and Figure 10 respectively.

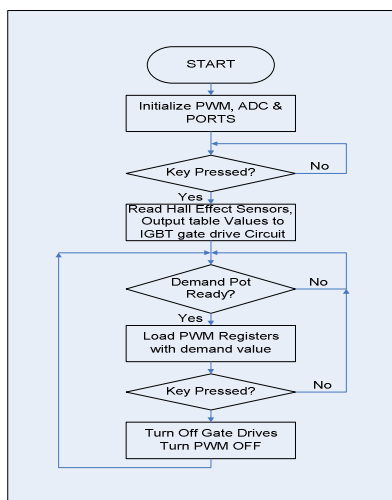


Figure 9: Flowchart of Open-Loop Controller

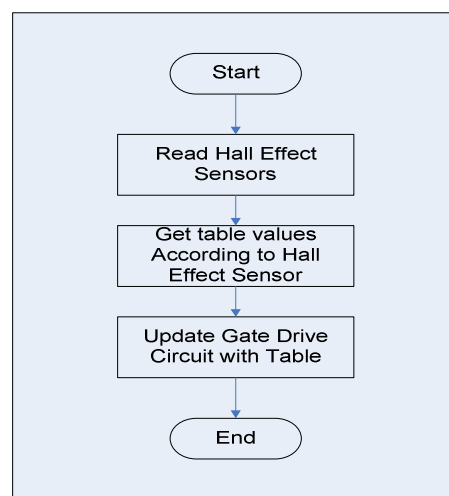


Figure 10: Flowchart of Change Notification Interrupt

7. Computer simulation

7.1 Simulation Methodology

The simulation was carried out using Ansoft Simplorer which has a built-in machine module PM Synchronous Machine. The module utilizes the equations derived below with machine parameters defined as in **Table I**. The three phase windings of the machine are distributed symmetrically to produce a phase shift of 120 degree with respect to each other. The state space equations are defined as follows [10, 11]:

$$\begin{bmatrix} i'_a \\ i'_b \\ \omega'_r \end{bmatrix} = \begin{bmatrix} -\frac{R_s}{L_s} & 0 & 0 \\ 0 & -\frac{R_s}{L_s} & 0 \\ 0 & 0 & -\frac{F}{J} \end{bmatrix} \begin{bmatrix} i_a \\ i_b \\ \omega_r \end{bmatrix} + \begin{bmatrix} \frac{2}{3L_s} & \frac{1}{3L_s} & 0 \\ -\frac{1}{3L_s} & \frac{1}{3L_s} & 0 \\ 0 & 0 & \frac{1}{J} \end{bmatrix} \begin{bmatrix} v_{ab} - E_{ab} \\ v_{bc} - E_{bc} \\ T_e - T_i \end{bmatrix} \quad (12)$$

$$\begin{bmatrix} i_a \\ i_b \\ i_c \\ \omega_r \end{bmatrix} = \begin{bmatrix} 1 & 0 & 0 \\ 0 & 1 & 0 \\ -1 & -1 & 0 \\ 0 & 0 & 1 \end{bmatrix} \begin{bmatrix} i_a \\ i_b \\ \omega_r \end{bmatrix} \quad (13)$$

The converter was modeled by six ideal switches with anti-parallel diodes and series resistances to simulate switch on resistance of the actual IGBT. The whole module was drawn using Simplorer as shown in **Figure 11**. The PWM module was implemented with a frequency of 16 kHz to match the actual converter and Rotor Angle. Hall Effect sensors were simulated using state machines in Simplorer as shown in **Figure 12**. The model was used to switch the related IGBT pair to rotate the motor in the right sequence. The Hall Effect sensors change its state every 60° electrical angle of the machine.

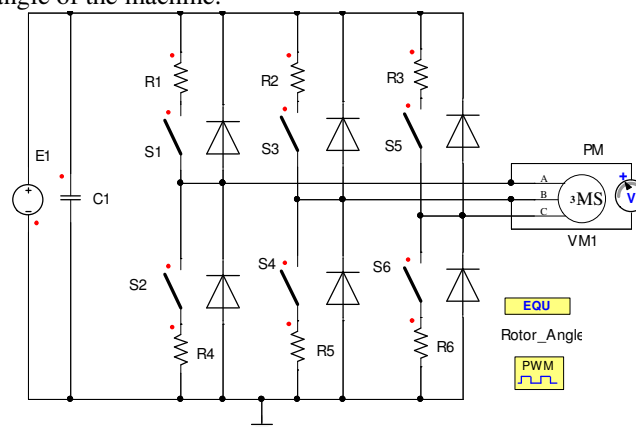


Figure 11: Power converter model in Simplorer

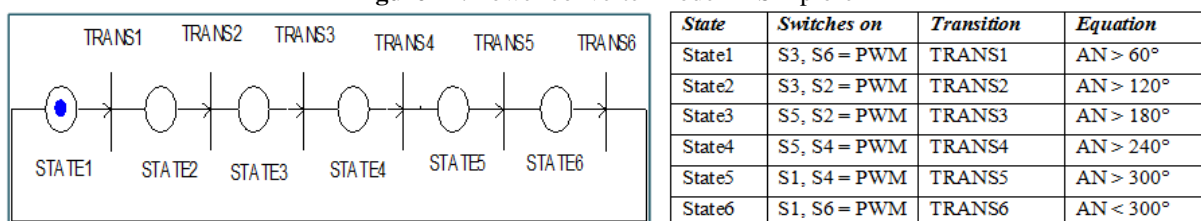
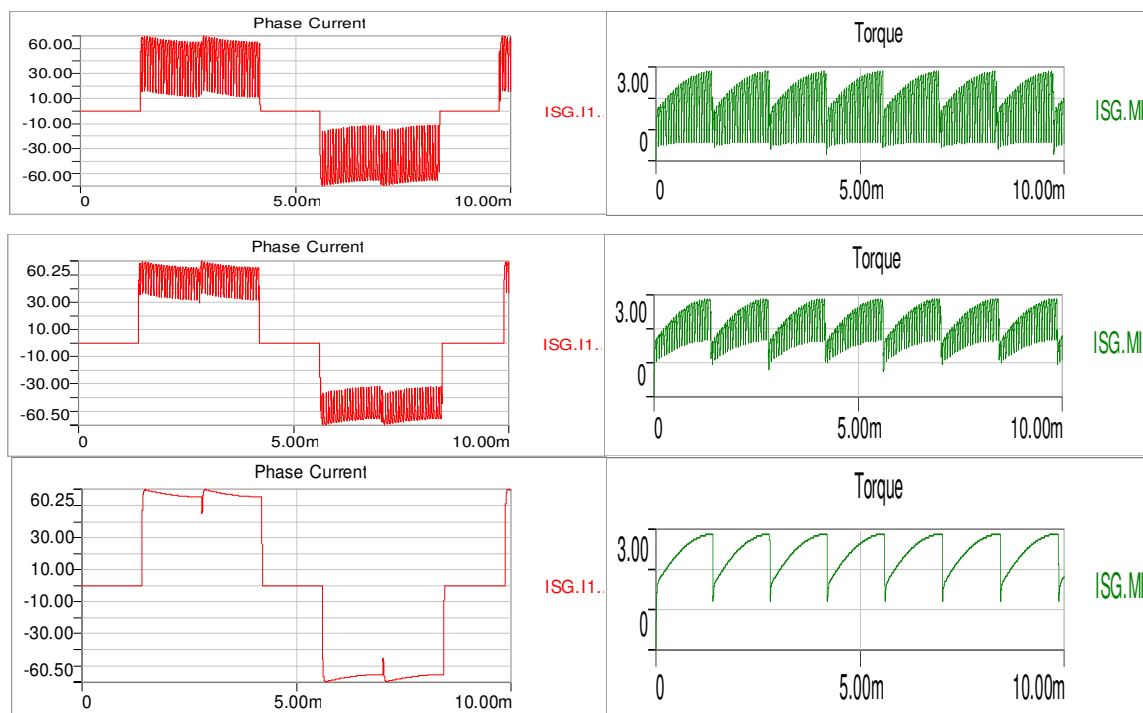


Figure 12: State Machines to simulate Hall Effect Sensors

7.2 Simulation Results

The simulation was carried out by setting the DC-link voltage to 83VDC which is the maximum voltage of the power supply used for the experimental setup. Results for the simulated phase current and its corresponding torque at various duty cycles are depicted in **Figure 13** to **Figure 15**. It can be seen from the simulated waveforms that the current and torque ripples are reduced at higher PWM duty cycles. Almost no current nor torque ripples produced at 100% duty cycle as seen in **Figure 15**.



8. Experimental Results

A basic test was conducted to obtain initial understanding of the behavior of the machine under various voltage, current and load conditions. This has enabled the design of appropriate open loop and closed loop controller that is capable of running the machine at the rated power and speed. The test rig for the AFPM machine is depicted in **Figure 16**.

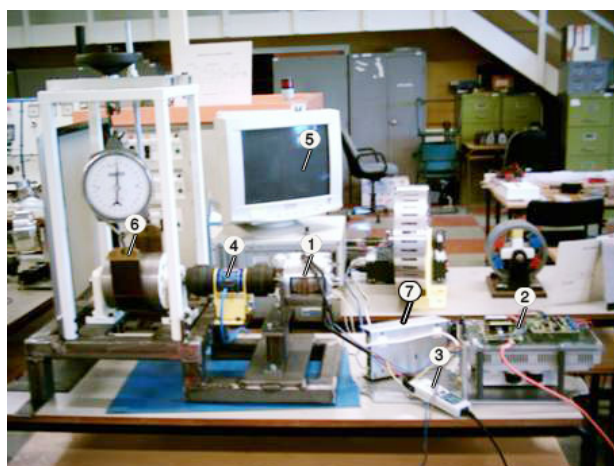
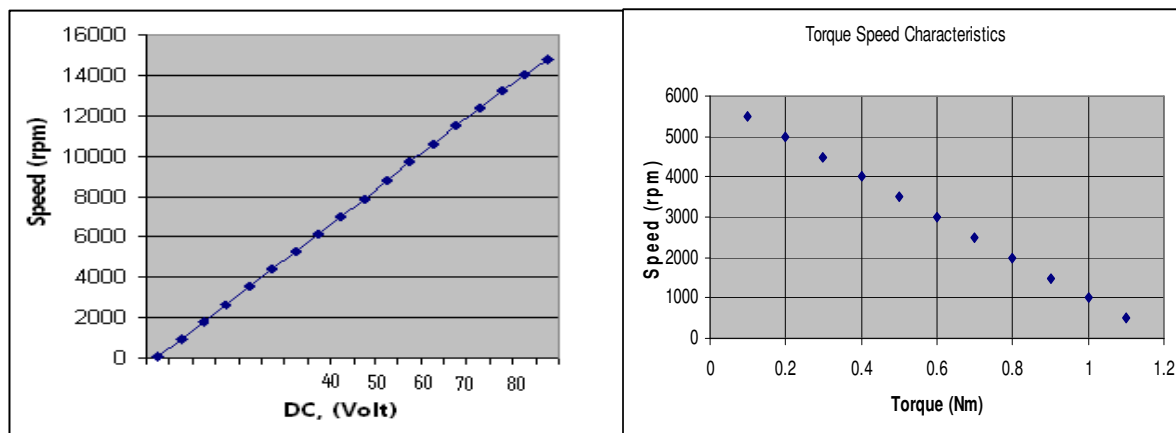


Figure 16: Test Rig fixture for experimental work where 1- high speed AFPM machine , 2 BLDC motor controller, 3- current probe, 4- torque sensor, 5- PC, 6 – friction load, 7- DC link power supply.

At this stage the No-load test was carried out by setting the DC-link voltage to 83VDC due to the power supply limitation. Initial experimental test result is depicted in **Figure 17-(a)**. It can be shown from the speed-voltage curve that speed of the machine is increased linearly with respect to DC link supply voltage which can be referred to the ironless stator construction of the machine.

The linear speed-voltage characteristics of the machine helps to predict the speed at higher supplied voltage using the linear extrapolation of the test results. Hence, a DC link supply voltage of 267 Volts is required to drive the AFPM machine at its rated speed of 50,000 rpm. The machine was then tested at various load conditions to obtain the torque-speed characteristics as well as the current waveforms at various duty cycles. Torque-speed result is also presented in **Figure 17-(b)** which shows a linear variation of torque with respect to

rotor speed. Such linear behavior also enables the extrapolation of the torque-speed results at the rated machine conditions.



To obtain the current waveforms under load condition, the machine was tested at several duty cycles starting from 90 % to 100 %. The torque load of 4 N.m was fixed while a maximum current of 60A was drawn at such a specific load. Results obtained for the current waveforms at 95 % and 100% of duty cycle are depicted in **Figure 18-(a)**, **Figure 18-(b)** respectively.

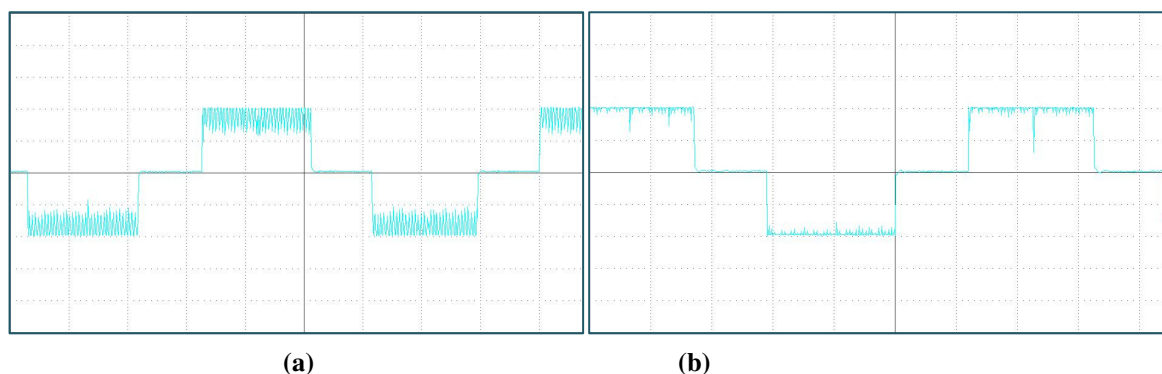


Fig. 18: Tested Phase Current waveform (60 Amps) @ speed = 3000 rpm and Torque Load = 4N.m (a) at PWM = 0.95, (b) at PWM = 1.

9. Conclusions and Recommendations

In this research a simple, low cost sensed control has been introduced for the control of High-speed AFPM machine. Theoretical model was developed and computer simulation was performed to obtain initial results for machine control performance. A low to medium speed test was conducted on the AFPM machine to validate the simulated results. Useful results were obtained from this research as the results showed a good match between the simulated and experimental results. It is shown that high ripples are produced in the current waveforms due to low winding inductances of the machine. However, such ripples are minimized at higher frequencies and duty cycle > 95%.

One of the challenges observed during the experimentation of the machine is the inaccurate positioning of the hall effect sensors since they were located in a confined spaces in the stator windings. One has to embed the sensors earlier during the molding and assembling of the stator windings to avoid any problems in the positioning and allocation of the hall sensors.

The linear behavior of the machine and the consistency of the simulated and experimental results unlock the potential for further investigations on the control strategies for such types of machines. Sensorless control need to be considered while running the machine at its rated speed and power. The future work on the machine may consider the following aspects:

- Provision of the DC link 0 – 300 V DC with rated current of 70 A to operate the machine at its rated power and speed.
- Exploration of the sensorless control design to eliminate the wires required for rotor position sensing.

References

- [1] K.R. Pullen, M.R. Etemad, and M.R. Fenocchi “The high speed axial flux disk generator unlocking the

potential of automotive gas turbine," IEE Colloquium on Machines and Drives for Electric and Hybrid Vehicles, pages 1—4, June 1996

- [2] El-Hasan, T.S.; Luk, P.C.K.; Bhinder, F.S.; Ebaid, M.S. "Modular design of high-speed permanent-magnet axial-flux generators," IEEE Transactions on Magnetics, Vol: 36 , Issue: 5 , Part: 1, Digital Object Identifier: 10.1109/20.908897, June 2000, pp. 3558 – 3561,
- [3] El-Hasan, T.S., Luk, P.C.K. "Magnet topology optimization to reduce harmonics in high-speed axial flux Generators," IEEE Transactions on Magnetics, Vol: 39 , Issue: 5 , Part: 2, Digital Object Identifier: 10.1109/TMAG.2003.816250, June 2003 , pp. 3340 – 3342.
- [4] Fei, W., Luk, P.C.K., El-Hasan, T.S. "Rotor Integrity Design for a High-Speed Modular Air-Cored Axial-Flux Permanent-Magnet Generator," IEEE Transactions on Industrial Electronics, Vol: 58 , Issue: 9, Digital Object Identifier: 10.1109/TIE.2011.2106097, Nov 2011 , pp. 3848 – 3858.
- [5] J. O. Kraha, J. Holtz "High-Performance Current Regulation and Efficient PWM Implementation for Low Inductance Servo Motors," IEEE Transactions on Industry Applications, Vol. 35, No. 5, Sep/Oct. 1999, pp. 1039-1049.
- [6] Krahenbuhl, D., Zwyssig, C., Kolar, J.W. "Half-Controlled Boost," Rectifier for Low-Power High-Speed Permanent-Magnet Generators," IEEE Transactions on Industrial Electronics, Vol: 58, Issue: 11, Digital Object Identifier: 10.1109/TIE.2011.2126531, 2011 , pp. 5066 – 5075.
- [7] Haoran Bai, "Study of PWM Rectifier/Inverter for a High Speed Generator," Power System, Power and Energy Engineering Conference (APPEEC), 2010 Asia-Pacific, Digital Object Identifier: 10.1109/APPEEC.2010.5449410, pp. 1 – 4.
- [8] A. Maamoun, Y. M. Alsayed, and A. Shaltout, "Space-Vector PWM Inverter Feeding a Permanent-Magnet Synchronous Motor," World Academy of Science, Engineering and Technology 41, 2010; pp. 627 – 631.
- [9] Z. Wang, J. Jin, Y. Guo, and J. Zhu, "SVPWM techniques and applications in HTS PMSM machines control," Journal of Electronic Science and Technology of China, vol. 6, no. 2, June 2008, pp. 191-197.
- [10] A. Tashakori, M. Ektesabi, and N. Hosseinzadeh "Modeling of BLDC Motor with Ideal Back-EMF for Automotive Applications", Proceedings of the World Congress on Engineering, Vol II, WCE2011 July 6 - 8, 2011, London, U.K.
- [11] Mohammed Naseeruddin, A.Mallikarjuna Prasad, "Analysis of the speed control of BLDC motor on matlab/simulink" National Conference On Electrical Sciences -2012 (NCES-12), ISBN: 978-93-81583-72-2